

Large-Scale Bayesian Causal Discovery with Interventional Data

Seong Woo Han¹, Daniel Duy Vo², and Brielin C. Brown^{*1,3,4}

¹Department of Computer and Information Science, University of Pennsylvania

²Genomics and Computational Biology Graduate Group, University of Pennsylvania

³Division of Informatics, University of Pennsylvania

⁴Department of Genetics, University of Pennsylvania

October 3, 2025

Abstract

Inferring the causal relationships among a set of variables in the form of a directed acyclic graph (DAG) is an important but notoriously challenging problem. Recently, advancements in high-throughput genomic perturbation screens have inspired development of methods that leverage interventional data to improve model identification. However, existing methods still suffer poor performance on large-scale tasks and fail to quantify uncertainty. Here, we propose Interventional Bayesian Causal Discovery (IBCD), an empirical Bayesian framework for causal discovery with interventional data. Our approach models the likelihood of the matrix of total causal effects, which can be approximated by a matrix normal distribution, rather than the full data matrix. We place a spike-and-slab horseshoe prior on the edges and separately learn data-driven weights for scale-free and Erdős–Rényi structures from observational data, treating each edge as a latent variable to enable uncertainty-aware inference. Through extensive simulation, we show that IBCD achieves superior structure recovery compared to existing baselines. We apply IBCD to CRISPR perturbation (Perturb-seq) data on 521 genes, demonstrating that edge posterior inclusion probabilities enable identification of robust graph structures.

1 Introduction

Inferring the causal relationships among a set of measured variables is one of the fundamental challenges of science (Bunge, 2012). These relationships are typically represented in a directed acyclic graph (DAG), with nodes representing variables and the presence of an edge from one variable to another indicating the former has a direct causal effect on the latter. Unfortunately the DAG is not identifiable from observational data alone (Verma and Pearl, 1990), and identifying the equivalence class of DAGs consistent with the data is NP-hard, making it intractable for problems involving even a modest number of variables (Chickering, 1996).

This issue has recently received substantial attention in genomics, where progress in understanding biological mechanisms of disease is now thought to hinge on understanding gene regulatory networks containing thousands of variables (Boyle et al., 2017; Liu et al., 2019; Wray et al., 2018). Fortunately, advances in CRISPR screening techniques such as Perturb-seq (Dixit et al., 2016; Gasperini et al., 2019; Montalbano et al., 2017) allow researchers to systematically perturb specific genes and measure the response, yielding *interventional* data for hundreds to thousands of genes measured in upwards of one-million cells (Replogle et al., 2022; Feng et al., 2024). This has created an ideal setting for the development of methods for inferring causal graphs at scale (Xue et al., 2023; Yang et al., 2018; Brown et al., 2023; Nazaret et al., 2023; Annadani et al., 2023; Hägele et al., 2023; Weinstock et al., 2024).

While differentiable causal discovery methods (Zheng et al., 2018; Brouillard et al., 2020; Nazaret et al., 2023; Lopez et al., 2022) have made tremendous advancements and received substantial attention, they are limited to returning a single optimal DAG without uncertainty quantification. In contrast, Bayesian methods (Madigan et al., 1995; Geiger and Heckerman, 2002; Friedman and Koller, 2003; Agrawal et al., 2018; Hägele et al., 2023; Annadani et al., 2023; Weinstock et al., 2024) aim to characterize the posterior distribution over possible graphs. This is critical as there may be multiple different near-optimal DAGs.

*Correspondence: brielin@upenn.edu

Uncertainty is also invaluable for scientific applications where assessing the degree of confidence in an edge or graph structure is required in order to prioritize follow-up investigations or experiments.

Due to the exponential scaling of the number of DAGs, exact posterior calculation is intractable for all but the smallest problems (Tian and He, 2009). Most practical approaches have therefore focused on using Markov Chain Monte Carlo (MCMC) to sample from the posterior (Geiger and Heckerman, 2002; Friedman and Koller, 2003; Agrawal et al., 2018), however these approaches do not accommodate intervention data. Recent work uses gradient information to further speed up inference (Annadani et al., 2023; Lorch et al., 2021; Cundy et al., 2021; Deleu et al., 2022; Toth et al., 2022, 2024), but these approaches still fail to scale to the volume of data we consider here.

We take an alternative approach. Rather than directly modeling the distribution of the DAG structure or direct edge weights given the data, we use the data to calculate the total causal effect (TCE) of every feature on every other. This reduces the amount of data that needs to be considered when calculating the likelihood. We then approximate the posterior distribution of the direct effect matrix given the total effect matrix. While modeling direct effects from total effects has been previously considered (Hyttinen et al., 2012; Brown et al., 2023; Weinstock et al., 2024), we present the first fully Bayesian treatment of this model and the first causal discovery method that scales to large problems while quantifying uncertainty. Moreover, while recent causal discovery approaches often model interventions, they typically assume *hard* or *structural* interventions which alter the DAG. We instead consider more realistic *soft* interventions, sometimes called *shift* interventions (Sani et al., 2020), that perturb targeted variables while leaving the structure in tact. We summarize our contributions as follows:

- We formulate the problem of inferring the DAG as finding the inverse of the TCE matrix in the linear-autoregressive model using soft interventions.
- We show that asymptotically normal estimators of the TCE entries lead to a sampling distribution that can be well-approximated by a matrix normal distribution. This substantially reduces the dimensionality of the sampling covariance and enables efficient likelihood-based inference.
- We propose a hybrid empirical Bayesian prior over the DAG by combining global sparsity patterns with edge specific weights optimized from covariance estimates in the observational data. We learn Erdős–Rényi (ER) and scale-free (SF) priors separately through structure-specific optimization, yielding a flexible, data-adaptive prior.
- We perform extensive empirical analyses while varying properties of the DAG, demonstrating superior performance to existing approaches combined with the ability to quantify uncertainty in edge inclusion.
- We assess uncertainty on real data by 1) performing a cross-validation analysis of 521 genes in the “essential” Perturb-seq screen (Replogle et al., 2022) and 2) performing an out of distribution replication analysis between the “essential” and independent “genome-wide” Perturb-seq screen, showing that posterior inclusion probabilities (PIPs) provide robust and practical measures of edge significance across folds and across datasets.

2 Background

2.1 Causal discovery

Causal discovery is the process of learning a causal graphical model (CGM), specifically a structural equation model (SEM), on a set of variables from data (Pearl, 2009). Formally, the model is represented by a DAG $\mathcal{G} = (V, E)$ where each node $i \in V$ corresponds to one of D variables $\{y_i\}_{i=1}^D$ and an edge $(i, j) \in E$ represents a direct effect of y_i on y_j . This is augmented by a set of functions detailing the relationship between each variable and its causal parents, $y_i = f_i(y_{pa_i^c}, \epsilon_i)$, where ϵ_i is an exogenous noise variable. Typically the variables $\{\epsilon_i\}_{i=1}^D$ are assumed random, unmeasured and independent, and we can equivalently specify the model in terms of probability distributions $p_i(y_i|y_{pa_i^c})$. Assuming causal sufficiency, *i.e.* that all other relevant variables are measured, this gives the causal model.

The data, \mathcal{D} , can be either purely observational, consisting of N measurements of the variables, $Y = [y_{ni}]_{n=1, i=1}^{N, D}$, or interventional. With interventional data, the measured variables are augmented by a binary indicator matrix $X = [x_{nm}]_{n=1, m=1}^{N, M}$, where $x_{nm} = 1$ if sample n received intervention m . These interventions

can be either *hard* (structural) or *soft* (shift). With hard interventions, incoming edges to the intervened-on variables are assumed to be broken, yielding a set of interventional distributions $p_{m_i}(x_i)$ for each $i \in \mathcal{I}_m$. With soft interventions, the distribution is changed without breaking the incoming connections, $p_{m_i}(x_i|y_{pa_i^G})$. The targets of the interventions $\{\mathcal{I}_m\}$ can be assumed to be known or unknown.

2.2 The linear-autoregressive causal model

While inferring the parents of each node pa_i^G and the full form of p_i for every variable y_i is an admirable goal, a more tractable goal in practice is to summarize the direct effect of one node on another in terms of an average causal effect. This motivates the approximation $f_j(y_{pa_j^G}, \epsilon_i) := \sum_i y_i G_{ij} + \epsilon_i$, where G_{ij} is the direct effect size of i on j . This gives the well-studied linear-autoregressive causal model that we consider here (Geiger and Heckerman, 2002; Hyttinen et al., 2012; Zheng et al., 2018; Brown et al., 2023; Weinstock et al., 2024),

$$Y = YG + \epsilon, \quad (1)$$

with $G = [G_{ij}]_{i=1, j=1}^{D, D}$ the weighted adjacency matrix encoding the graph.

2.3 Bayesian causal discovery

In Bayesian causal discovery, the goal is to estimate the entire posterior distribution of CGMs given the data, $p(\mathcal{G}, \Theta | \mathcal{D})$, where Θ parameterizes the conditional distributions p_i (Friedman and Koller, 2003). This requires prior distributions over DAGs $p(\mathcal{G})$ and parameters $p(\Theta | \mathcal{G})$, and a likelihood $p(\mathcal{D} | \mathcal{G}, \Theta)$, so that Bayes rule can be applied to yield the posterior. Under the linear auto-regressive model the prior and likelihood can be expressed in terms of the weighted adjacency matrix,

$$p(G | \mathcal{D}) \propto p(\mathcal{D} | G) p(G). \quad (2)$$

The posterior encapsulates epistemic uncertainty regarding the structure of the graph given the data. Due to the sheer number of possible graph structures in the posterior, we focus here on summarizing the posterior through the posterior mean graph, which we define as the average weighted adjacency matrix $\mathbb{E}[G | \mathcal{D}]$, and the posterior inclusion probability of each edge,

$$\text{PIP}_{ij} = \Pr(|G_{ij}| > \varepsilon | \mathcal{D}), \quad (3)$$

where ε is a small edge-existence threshold.

2.4 Instrumental variables and soft interventions

When interventions are assumed to be hard, the interventional distribution is typically specified by removing the dependency of the intervened node on its parents, $p_{m_i} = p_{\epsilon_i}$, or by fixing it to a specific value such as 0, $\text{do}(y_i = 0)$. If the intervention instead results in a weak perturbation to its target, the interventional distribution is more difficult to specify, but is commonly modeled as a mean shift (Sani et al., 2020). An alternative approach is to treat the interventions as instrumental variables (IVs). x is a valid IV for y_i on y_j if x is not independent of y_i and if x is independent of all exogenous factors affecting y_j given $\text{do}(y_i)$ (Pearl, 2000). Thus in our model an intervention \mathcal{I}_m targeting variable y_m is trivially an IV for y_m on every other variable $y_{i \neq m}$.

While there are many techniques for instrument variables analysis (Levis et al., 2024; Imbens, 2014; Baiocchi et al., 2014), the simplest to consider in the linear case given here is two-stage least squares (2SLS). In 2SLS, the average casual effect $\mathbb{E}[y_j | \text{do}(y_i)] = R_{ij} y_i$ is estimated by regressing y_i on the instrument(s) x to get \hat{y}_i , then regressing y_j on \hat{y}_i ,

$$\hat{R}_{ij} = (Y_i^\top P_x Y_i)^{-1} P_x Y_i^\top Y_j \quad (4)$$

with $P_x = x(x^\top x)^{-1} x^\top$ the projection matrix onto the column space of x . Note that this measures the *total* causal effect of y_i on y_j under the model G , not the direct effect. Letting $\mathcal{P}_{i \rightarrow j}^G$ be the set of paths connecting y_i and y_j in G , we can write R_{ij} as the sum of the product of the edge values in each path, $R_{ij} = \sum_{p \in \mathcal{P}_{i \rightarrow j}^G} \prod_{(k, l) \in p} G_{kl}$ (Hyttinen et al., 2012).

Hard interventions. While our focus is on soft interventions, we note that the same pipeline can accommodate hard interventions. For an intervention \mathcal{I}_m with target y_i , form $G^{(m)}$ by zeroing column m of G and write

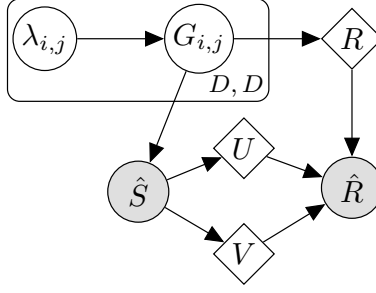


Figure 1: The IBCD model. We treat \hat{R} and \hat{S} as observed and model \hat{R} as coming from a matrix normal distribution $\mathcal{MN}(R, U, V)$ with U and V determined from \hat{S} . We place a spike-and-slab horseshoe prior on G which determines the mean matrix R via (6).

$Y^{(m)} = Y^{(m)}G^{(m)} + c^{(m)} + \varepsilon^{(m)}$. In this regime y_i is exogenous, so the total effect on y_j is identified from the intervened samples by ordinary least squares, $\hat{R}_{ij} = (Y_i^{(m)\top} Y_i^{(m)})^{-1} Y_i^{(m)\top} Y_j^{(m)}$.

3 Interventional Bayesian Causal Discovery

3.1 Data model

We augment the standard linear-autoregressive model (1) with soft interventions,

$$Y = YG + X\beta + \epsilon, \quad (5)$$

where Y and X are the $N \times D$ and $N \times M$ data and intervention design matrices as before, β is the $M \times D$ matrix of unknown intervention on gene effects, and ϵ is an $N \times D$ exogenous noise matrix.

We assume that the direct targets of the interventions are known but that the effects of the interventions are unknown. That is, we know which entries of β are non-zero but not their values. This is a reasonable assumption in Perturb-seq data where the CRISPR guide target is known and off-target effects are minimal (Replegle et al., 2022). We also assume that every feature has at least one instrument so that every element in the matrix \hat{R} can be estimated. We assume that the exogenous variables ϵ_i are independent with bounded variance, but make no other assumptions about their distributions p_{ϵ_i} . R can also be written recursively,

$$\begin{aligned} R &= \left[\sum_k R_{ik} G_{kj} \right]_{i=1, j=1}^{D, D} \\ &= \sum_{d=0}^{\max\{|p|, p \in \mathcal{P}^G\}} G^d = (I - G)^{-1} \end{aligned} \quad (6)$$

This together with collecting terms of (5) and multiplying by the inverse yields the model,

$$Y = (X\beta + \epsilon)(I - G)^{-1} = X\beta R + \epsilon R. \quad (7)$$

3.2 Empirical Bayesian model

Our approach is inspired by a common strategy in genome-wide association studies, where it is typically more computationally efficient to work with summary statistics of the data, effect sizes and their standard errors, rather than the full data matrix (Pasaniuc and Price, 2017). Thus, instead of modeling Y , we use Y and X to estimate the total effects \hat{R}_{ij} and their covariances $\hat{S}_{ijkl} = \text{Cov}(\hat{R}_{ij}, \hat{R}_{kl})$. We then model \hat{R} with a matrix normal likelihood and place a horseshoe mixture prior on G . See Figure 1 for an overview plate diagram.

Matrix normal likelihood. If the instrumental variables estimator has a normal distribution asymptotically, the likelihood $p(\hat{R} | G, \hat{S})$ can be approximated by a matrix normal $\mathcal{MN}(R, U, V) = \mathcal{MN}((I - G)^{-1}, U, V)$. Recall that $X \sim \mathcal{MN}_{n \times p}(M, U, V)$, if $\text{vec}(X) \sim \mathcal{N}_{n \cdot p}(\text{vec}(M), V \otimes U)$, where \otimes denotes the Kronecker

product. Here, $U \in \mathbb{R}^{n \times n}$ captures row-wise correlations, $V \in \mathbb{R}^{p \times p}$ captures column-wise correlations, and $S = V \otimes U$ defines the full $np \times np$ covariance matrix. In our model, U captures the covariances $\hat{S}_{i,k}$ between interventions on variables induced by the design matrix X , and V captures the covariances $\hat{S}_{j,l}$ between the response of variables to interventions. This reduces the computational burden of estimating D^4 entries in the covariance matrix \hat{S} to estimating the $2D^2$ entries in the covariance matrices U and V .

Estimating the matrix normal covariance matrices. For linear IV estimators, the entries of the variance-covariance matrix \hat{S} are given by (Appendix A),

$$\hat{S}_{ijkl} = \frac{\text{Cov}(\hat{y}_i, \hat{y}_k) \text{Cov}(\hat{\epsilon}_{ij}, \hat{\epsilon}_{kl})}{n \text{Var}(\hat{y}_i) \text{Var}(\hat{y}_k)}, \quad (8)$$

where n is the total number of observations, \hat{y}_i is the projection of y_i onto the space spanned by its instruments, and $\hat{\epsilon}_{ij} = Y_j - \hat{R}_{ij} Y_i$ is an estimate of the residual. Notice a natural separation into two terms, the first representing covariation of the projections onto the instrument sets X_i and X_k , and the second representing covariation in the response of y_j and y_l to upstream interventions. While this response is dependent on the intervened variables, we average over interventions to approximate the the matrix-normal column covariance. As such we can write,

$$\hat{U}_{ik} = \frac{\text{Cov}(\hat{y}_i, \hat{y}_k)}{n \text{Var}(\hat{y}_i) \text{Var}(\hat{y}_k)}, \quad (9)$$

$$\hat{V}_{jl} = \frac{1}{\sum_{ik} \mathbb{1}\{U_{ik} \neq 0\}} \sum_{i,k|U_{ik} \neq 0} \text{Cov}(\hat{\epsilon}_{ij}, \hat{\epsilon}_{kl}), \quad (10)$$

where $\mathbb{1}\{U_{ik} \neq 0\}$ indicates non-zero entries in U which are known through the intervention design matrix X .

Learning priors in sequence We specify an empirical Bayes Spike and slab horseshoe prior over G informed by the structure of the data, $p(G | \hat{S})$. We assume each direct effect G_{ij} follows a unimodal distribution centered at zero. We first fit a global inclusion prior in the ER or SF form depending on structural assumptions to obtain marginal edge inclusion probabilities. We then localize these probabilities to edges and finally use them to parameterize the spike and slab horseshoe prior governing the edge weights.

Learning ER prior. To capture ER structure, we estimate marginal edge inclusion probabilities with a mixture Gaussian to the observed effects \hat{R} (Stephens, 2017). This flexible empirical Bayes prior captures both sparsity and heterogeneous effect sizes while remaining computationally stable compared to traditional spike and slab formulations. Details of the mixture specification and the Expectation Maximization (EM) estimation for the spike and slab weights are provided in Appendix B.

Learning SF prior. To capture SF structure, we derive edge inclusion probabilities from the squared total effect matrix $A = |\hat{R}|^2$, which amplifies strong signals and suppresses noise. We compute empirical out-weights $\theta_i = \sum_{j \neq i} A_{ij}$ and in-weights $\phi_j = \sum_{i \neq j} A_{ij}$, and solve the constrained optimization

$$\min_{P_{ij} \in [0,1], i \neq j} \sum_{i=1}^D \left(\sum_{j \neq i} P_{ij} - \theta_i \right)^2 + \sum_{j=1}^D \left(\sum_{i \neq j} P_{ij} - \phi_j \right)^2 \quad (11)$$

subject to $P_{ii} = 0$, to recover a probabilistic edge inclusion matrix $P \in [0, 1]^{D \times D}$. We then transform the solution into spike weights $\pi_{0,ij} = 1 - P_{ij}$.

Localizing the global prior. Assuming faithfulness (Vonk et al., 2023), two variables with a causal effect between them cannot be statistically independent. As such, we capture the intuition that more correlated variables are more likely to reflect a causal effect *a priori* by building an edge specific prior, $p(G_{ij}) \propto \text{Cov}(y_i, y_j)$ in the observational (non-intervened) data. Together, this hybrid empirical Bayes strategy leverages both global patterns and local signal to construct a structured, data-driven prior over G that improves both precision and interpretability in causal network inference, see Appendix B for details.

Spike-and-slab horseshoe prior After learning edge specific spike and slab weights separately from the ER and SF priors, we place a prior on each off-diagonal edge G_{ij} in the form of a non-centered spike-and-slab horseshoe:

$$G_{ij} \sim \pi_{0,ij} \mathcal{N}(0, \sigma_0^2) + (1 - \pi_{0,ij})(\tau \lambda_{ij} \epsilon_{ij}), \quad (12)$$

where $\sigma_0^2 = 10^{-3}$, $\epsilon_{ij} \sim \mathcal{N}(0, 1)$, $\lambda_{ij} \sim \text{HalfCauchy}(1)$, and $\tau = 0.1$. We use the non-centered reparameterization (Papaspiliopoulos et al., 2007) $\theta_{ij} = \tau \lambda_{ij} \epsilon_{ij}$ of the hierarchical horseshoe $\theta_{ij} \sim \mathcal{N}(0, \tau^2 \lambda_{ij}^2)$, where τ is a global shrinkage parameter and λ_{ij} provides local adaptivity. This reparameterization decouples latent variables from their scales and mitigates Neal’s funnel (Neal, 2003) for faster and more stable convergence.

Sampling from the posterior. Together, these components define the posterior,

$$p(G | \hat{R}, \hat{S}) \propto p(\hat{R} | G, \hat{S}) p(G | \hat{S}). \quad (13)$$

Our non-centered horseshoe prior produces a geometry that is well-suited for gradient-based inference. We perform inference using the No-U-Turn Sampler (NUTS) (Hoffman et al., 2014), implemented in NumPyro (Bingham et al., 2019; Phan et al., 2019), which leverages gradient information to scale inference to high-dimensional models, see Appendix C for details.

4 Experiments

We performed comprehensive evaluations of our method as compared to others on both simulated and real data. For simulation, we generated datasets, with a known intervention design matrix, from the model (7) using ER and SF DAGs varying dimensions, $D \in \{50, 150, 250, 500\}$. Each dataset included $N = 100$ intervention samples per variable and $D \times 100$ control samples, yielding $2D \times 100$ total observations. This choice of $N = 100$ conservatively matches the average of 141 cells per gene in the Replogle et al. (2022) Perturb-seq experiment. In addition, for $D = 50$ we conducted experiments with varying intervention sample sizes, $N \in \{5, 15, 25, 50, 75, 100\}$, under the same design. For real data we analyzed normalized single cell Perturb seq expression matrices from K562 spanning the genome wide and essential gene screens. We retained 521 genes well-captured in both studies for downstream analysis after regressing out S and G2M cell cycle effects, see Appendix D for details. We compare the posterior mean weighted adjacency matrix inferred by IBCD, obtained by averaging marginal edge weights across posterior samples, against various methods including NOTEARS (Zheng et al., 2018), SDCD (Nazaret et al., 2023), BayesDAG (Annadani et al., 2023), LiNGAM (Shimizu et al., 2006), GIES (Hauser and Bühlmann, 2012), GES (Chickering, 2002), inspre (Brown et al., 2023), and LLCB (Weinstock et al., 2024). To ensure a fair comparison, we applied the same thresholding rule to binarize adjacency matrices across all methods, and for purely observational methods (GES, NOTEARS, LiNGAM, BayesDAG) we doubled the number of control samples to match the total sample size of interventional datasets. Further experiment details are provided in Appendix D.

4.1 Scaling with dimension on synthetic ER and SF graphs

We evaluated each method by comparing the inferred graph to the ground truth using F1 score and structural Hamming distance (SHD). We compared all methods on synthetic datasets with known ground truth graphs averaged over ten replicates based on independently generated graphs and data. Figure 2 summarizes F1 and SHD for $D \in \{50, 150, 250, 500\}$ on ER and SF graphs. All optimization and score-based methods scaled to $D = 500$ except NOTEARS which ran to $D = 250$, while Bayesian methods LLCB and BayesDAG exceeded practical time or memory limits beyond $D = 50$, see Table 2 for details. IBCD achieves the best overall performance, with the highest average F1 score and lowest average SHD in both ER and SF graphs, highlighting the benefit of learning a prior that adapts to the underlying graph topology. Detailed per- D tables for F1, SHD, precision, and recall are provided in Tables 4 and 5, and Figures 7 and 8 in Appendix F.

Regarding performance of other methods, NOTEARS and inspre perform better on ER graphs, consistent with theory that says ℓ_1 -regularized methods need more samples to recover hub-heavy SF topologies (Liu and Ihler, 2011). By contrast, LiNGAM and SDCD are stronger on SF graphs. LiNGAM first estimates an ordering via independence tests, which we suspect may be easier when a few hubs dominate, and SDCD’s spectral-radius penalty seems numerically more stable on SF structures. GIES, the interventional extension of GES, outperforms GES, highlighting the benefit of using interventional data, though on SF graphs the gain diminishes and can vanish as D increases. We suspect that GES-family methods tend to do better on

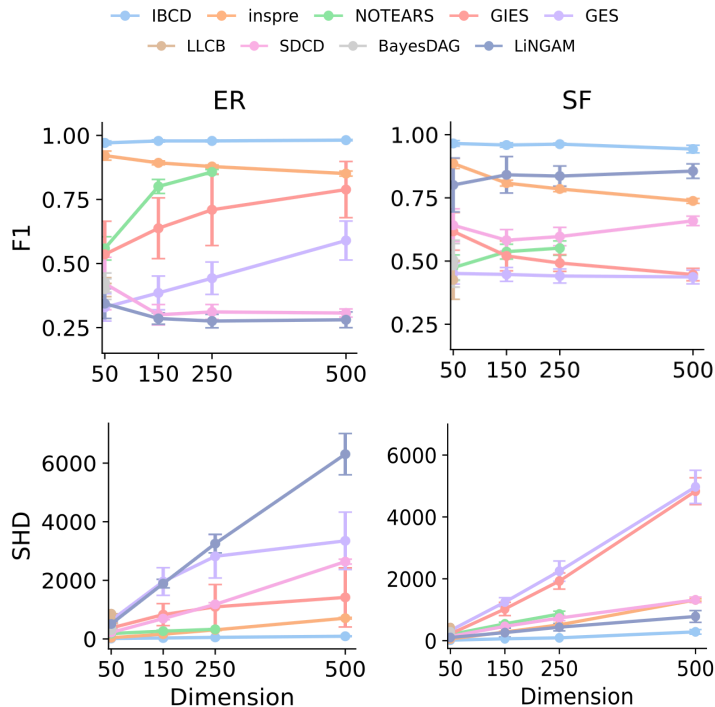


Figure 2: Comparison of F1 and SHD with increasing numbers of dimensions on ER and SF graphs, using 100 intervention samples per variable.

Variant	Empirical prior	MN	Edge specific	MVN	Global Prior	ER prior	SF prior	F1	SHD
ER baseline	✓	✓	✓	×	×	✓	×	0.875 ± 0.023	58.9 ± 10.10
Oracle Prior	×	✓	✓	×	×	✓	×	0.876 ± 0.017	59.9 ± 9.02
MVN Likelihood	✓	×	✓	✓	×	✓	×	0.431 ± 0.017	625.4 ± 18.75
Global Prior	✓	✓	×	×	✓	✓	×	0.845 ± 0.016	72.6 ± 6.06
ER with SF Prior	✓	✓	✓	×	×	×	✓	0.908 ± 0.017	44.5 ± 8.34
SF baseline	✓	✓	✓	×	×	×	✓	0.894 ± 0.020	47.6 ± 8.44
SF with ER Prior	✓	✓	✓	×	×	✓	×	0.809 ± 0.025	83.2 ± 11.42

Table 1: Ablation study results comparing mean and standard deviation of F1 and SHD metrics across model variants averaged over 10 replicates of 50D ER graph. ✓ indicates the presence of each component. MN indicates matrix normal, MVN indicates multivariate normal, ER indicates Erdős–Rényi, and SF indicates Scale-Free.

ER than SF graphs because ER graphs have a more even degree distribution, so the score may change more smoothly with edge edits, yielding fewer near-ties and more reliable greedy steps. In contrast, SF hubs may create many colliders and dense neighborhoods, which yields many near equivalent choices and makes greedy search more prone to suboptimal moves. More formal analysis would be required to validate this intuition.

4.2 Scaling with sample size at $D = 50$

We again assess performance with F1 and SHD, now varying the number of intervention samples per variable N at fixed dimension $D = 50$ for both ER and SF graphs (Figure 3). As N increases, most methods gain in F1 and drop in SHD with diminishing returns beyond about $N = 50$. IBCD achieves the best overall performance on ER and SF graphs, achieving the highest mean F1 and lowest SHD in almost all settings, except the low-sample case ($N = 5$). Detailed per- N tables for F1, SHD, precision, and recall are provided in Tables 6 and 7, and Figures 9 and 10 in Appendix F.

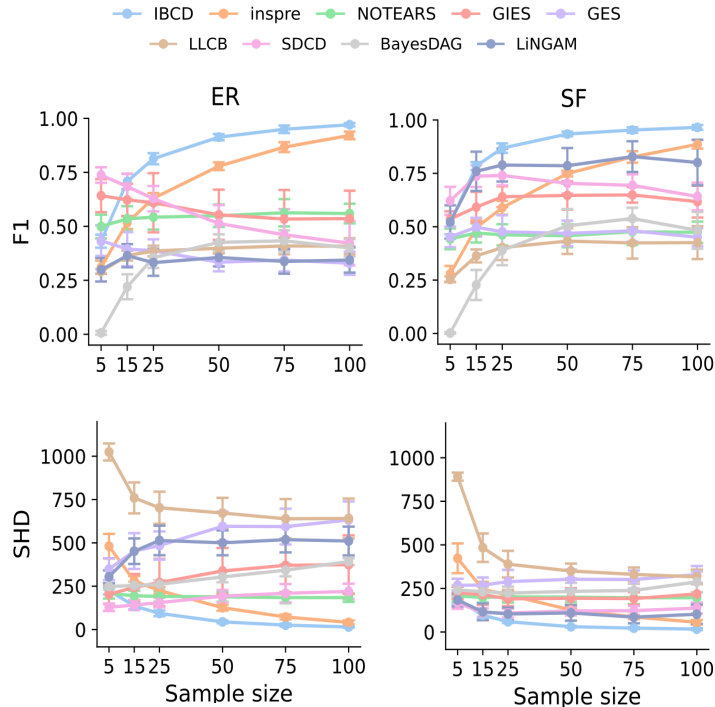


Figure 3: Comparison of F1 and SHD with increasing numbers of intervention sample sizes on ER and SF graphs with $D = 50$.

4.3 Ablation studies

To assess the contribution of each modeling component, we conducted ablation studies comparing different configurations on $D=50$ synthetic ER and SF graphs in Table 1 (see Appendix D). The ER baseline learns an empirical prior from \hat{R} with a matrix normal likelihood and edge specific weights. An oracle prior that uses the true graph gives only a small, statistically insignificant gain, showing that the observational summary \hat{R} provides a strong empirical prior (see Appendix E). To validate the likelihood we replaced the matrix normal with a multivariate normal that uses a truncated singular value decomposition of the covariance S keeping the top $r = 10$ components which reduces cost from $\mathcal{O}(D^3)$ to $\mathcal{O}(Dr^2)$ but reduced performance highlighting that learning structured row and column covariance matters. Using a single global prior also hurt which supports the value of edge specific priors obtained by localizing the global prior, highlighting the value of adaptive sparsity. Surprisingly, using an SF prior on ER graphs improves performance at $D = 50$ but degrades as D grows to 150, 250, and 500 with large drops in F1 and increases in SHD (Table 3, Appendix F). In contrast, the SF baseline outperforms SF with an ER prior, indicating that when the topology is unknown the SF baseline is a safer default.

4.4 Posterior edge confidence diagnostics on 500 nodes graphs

To verify that our $D = 500$ inference is not only scalable but also trustworthy at the edge level, we analyzed posterior inclusion probability (PIP) (3), with $\epsilon = 0.05$. The PIP quantifies posterior support for the presence of the edge. If PIPs are appropriately calibrated, approximately 80% of edges with $\text{PIP} = 0.80$ represent true direct causal effects. Figure 4 shows that our reported PIPs are conservative for both ER and SF graphs in high-dimensional settings. Thus, PIPs can be used to assess confidence in individual edges even in difficult inference regimes.

4.5 Analysis of real Perturb-seq data

Finally, we sought to assess the performance of IBCD on real data. As there is a scarcity of large-scale data with ground truth causal graphs, we used five-fold stratified cross validation on 521 genes in the essential and

Dim	Sample	IBCD	inspre	GIES	GES	LiNGAM	SDCD	NOTEARS	BayesDAG	LLCB
50D	5	2m 59s	16s	1.3s	0.6s	1.4s	30s	37s	1m 52s	10h 17m
50D	15	3m 08s	15s	0.8s	0.9s	2.6s	1m 17s	53s	2m 49s	10h 37m
50D	25	3m 47s	15.7s	0.9s	1.1s	3.8s	2m 06s	1m 14s	3m 37s	10h 41m
50D	50	4m 11s	14.9s	2.1s	1.4s	6.9s	3m 49s	2m 06s	4m 58s	11h 24m
50D	75	4m 58s	14.8s	2.5s	4.1s	10.8s	5m 17s	3m 18s	5m 59s	10h 13m
50D	100	6m 20s	15.4s	2.0s	1.9s	14.2s	6m 46s	3m 34s	7m 07s	10h 39m
150D	100	14m 30s	4m 41s	37s	46s	5m 03s	26m 09s	1h 10m	NA	NA
250D	100	24m 27s	19m 41s	2m 25s	3m 28s	22m 02s	50m 05s	2h 30m	NA	NA
500D	100	45m 38s	2h 21m	20m 15s	41m 59s	2h 55m	1h 43m	NA	NA	NA

Table 2: Runtimes averaged across 10 replicates per setting, aggregated over ER and SF. All methods ran on a shared compute cluster with Intel Xeon E5-2660 v2 CPUs. IBCD and SDCD, the GPU-enabled methods, used NVIDIA H100 GPUs (80 GB VRAM each); IBCD leveraged three GPUs to parallelize MCMC sampling across chains. NA values correspond to failed runs, typically due to a 12 h timeout or termination for exceeding resource limits.

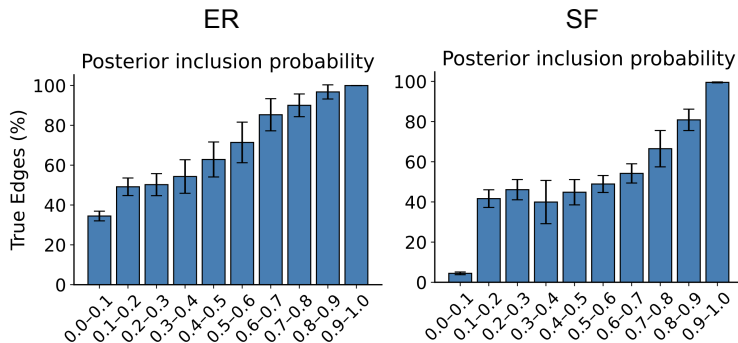


Figure 4: Calibration of posterior inclusion probability on 500D graphs under ER (left) and SF (right) graph in Figure 2. Bars show mean \pm s.d. over ten replicates. True edges concentrate in high PIP, confirming reliable uncertainty quantification.

genome-wide Perturb-seq screens (Replogle et al., 2022). For each fold $f \in \{1, \dots, 5\}$, we fit the model on the training cells and computed $\text{PIP}^{(f)}$ on the held-out cells. The scatter plot in Figures 5 and 11 overlays all ten unordered fold pairs $(\text{PIP}^{(i)}, \text{PIP}^{(j)})$ ($i < j$) for the GWPS and essential screens, respectively. Each point is one putative edge, axes are on a log scale, and the top panel shows the marginal distribution of PIP values. Both figures show that the global Pearson correlation across the ten fold pairs is higher with the SF prior ($r = 0.850$) than with the ER prior ($r = 0.687$). This is consistent with hub-dominated, heterogeneous gene regulatory networks, so a SF prior better matches the data. Adapting the prior to the topology improves the reproducibility of edge-level PIPs across sub-samples and supports the reliability of our 521-gene inference.

As the genome-wide and essential screens represent independent experiments with inevitable differences in unmeasured exogenous factors, we conducted an out of distribution validation experiment comparing the edge PIPs in both experiments. We fit IBCD on each full dataset and obtained posterior inclusion probabilities for all edges. We then compared PIP from the genome wide screen with PIP from the essential screen and observed a strong positive correlation ($r = 0.570$ for the SF prior, Figure 6). Again the correlation is much higher with an SF prior than with an ER prior which is consistent with hub dominated gene regulation in these cells.

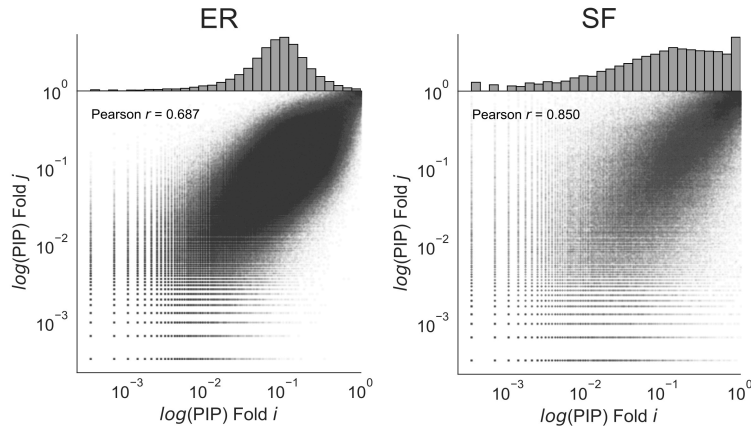


Figure 5: Agreement of log-transformed PIP across the ten cross-validation fold pairs on the K562 GWPS screen under ER and SF priors. Each point is one edge; the density of points forms a grey cloud. The positive correlation shows that high-PIP edges are consistently identified across folds.

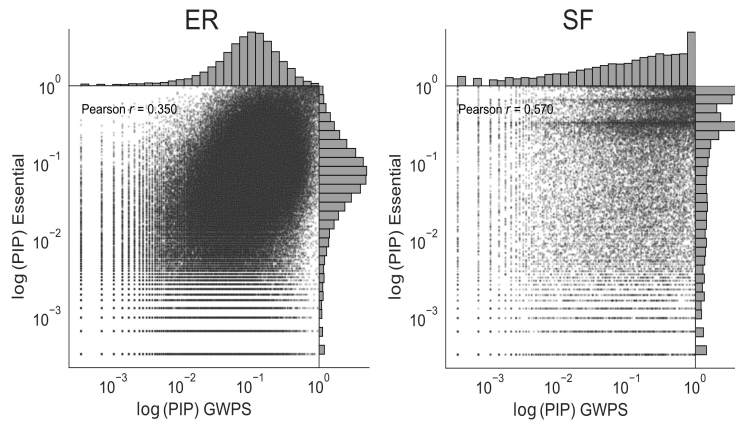


Figure 6: Agreement of log PIP values between GWPS and Essential K562 screens under ER and SF priors. Each point is one edge and darker regions indicate higher density. The SF prior shows stronger cross screen consistency.

5 Discussion

We have introduced Interventional Bayesian Causal Discovery (IBCD), an empirical Bayesian framework that scales Bayesian causal inference to hundreds of nodes while providing calibrated edge level uncertainty. IBCD departs from most existing work in two key ways. First, we treat experimentally perturbed variables as instruments using a soft intervention framework and summarize the data by the matrix of total causal effects, allowing a matrix normal likelihood that reduces the computational burden of likelihood evaluation by orders of magnitude. Second, we learn a spike-and-slab horseshoe prior, with data-driven global sparsity and edge specific weights adapted to the local covariance structure in the observational samples. We also fit topology aware priors separately for ER and SF regimes, allowing the learned prior to match the graph family while using the same inference engine. Third, we show that PIP estimates are stable across cross validation folds and highly correlated across independent experiments, with stronger correlation under the SF prior. This indicates that IBCD yields reproducible edge probabilities on real interventional data at scale.

However, the present work has several limitations that point toward clear avenues for improvement. First, we make several assumptions. Perhaps the most limiting is the assumption of a linear model. While non-linearities are sure to exist, the linear model is well-studied and represents the classic tradeoff between expressivity and tractability. We also assume that every variable has at least one instrument. While these types of large-scale screens are becoming common in genomics, this limits applicability in scenarios where

interventions are more difficult. Second, while we make no assumption on the distribution of error terms, we do assume that the IV estimator used to produce causal effect estimates is asymptotically normal. Relatedly, we focus on two-stage least-squares for IV estimates for simplicity, which assumes independence between the instrument and confounders that might not hold in practice. However, note that this framework allows any IV estimator with an asymptotic normal distribution to be used instead. Finally, our aim is to summarize the posterior via the mean graph and quantify edge level uncertainty through PIPs, rather than to characterize the full posterior. This enables straightforward comparisons with non-Bayesian methods but leaves important questions regarding the modal distribution of the posterior open. We hope to leverage multi-path approaches in future work to further characterize the posterior.

By providing scalable, uncertainty aware causal discovery, IBCD can help prioritize high confidence direct causal effects. This can inform experimental follow-up while flagging those that remain ambiguous, thereby reducing costly false leads or guiding experimental design to clarify ambiguous connections. More broadly, we have demonstrated that the combination of instrumental variable summaries with empirical Bayes shrinkage is a powerful, efficient approach to causal discovery with high-dimensional intervention data.

References

- Agrawal, R., Uhler, C., and Broderick, T. (2018). Minimal I-MAP MCMC for Scalable Structure Discovery in Causal DAG Models. In *Proceedings of the 35th International Conference on Machine Learning*, pages 89–98. PMLR. ISSN: 2640-3498.
- Annadani, Y., Pawlowski, N., Jennings, J., Bauer, S., Zhang, C., and Gong, W. (2023). Bayesdag: Gradient-based posterior inference for causal discovery. *Advances in Neural Information Processing Systems*, 36:1738–1763.
- Baiocchi, M., Cheng, J., and Small, D. S. (2014). Instrumental variable methods for causal inference. *Statistics in medicine*, 33(13):2297–2340.
- Bingham, E., Chen, J. P., Jankowiak, M., Obermeyer, F., Pradhan, N., Karaletsos, T., Singh, R., Szerlip, P., Horsfall, P., and Goodman, N. D. (2019). Pyro: Deep universal probabilistic programming. *Journal of machine learning research*, 20(28):1–6.
- Boyle, E. A., Li, Y. I., and Pritchard, J. K. (2017). An Expanded View of Complex Traits: From Polygenic to Omnigenic. *Cell*, 169(7):1177–1186. Publisher: Elsevier.
- Brouillard, P., Lachapelle, S., Lacoste, A., Lacoste-Julien, S., and Drouin, A. (2020). Differentiable causal discovery from interventional data. *Advances in Neural Information Processing Systems*, 33:21865–21877.
- Brown, B. C., Morris, J. A., Lappalainen, T., and Knowles, D. A. (2023). Large-scale causal discovery using interventional data sheds light on the regulatory network architecture of blood traits. *bioRxiv*.
- Bunge, M. (2012). *Causality and Modern Science: Third Revised Edition*. Courier Corporation. Google-Books-ID: YKkhLwpH09YC.
- Chickering, D. M. (1996). Learning Bayesian Networks is NP-Complete. pages 121–130. Publisher: Springer, New York, NY.
- Chickering, D. M. (2002). Optimal structure identification with greedy search. *Journal of Machine Learning Research*, 3:507–554.
- Clark, C. E. (1962). Letter to the editor—the pert model for the distribution of an activity time. *Operations Research*, 10(3):405–406.
- Cundy, C., Grover, A., and Ermon, S. (2021). Bcd nets: Scalable variational approaches for bayesian causal discovery. *Advances in Neural Information Processing Systems*, 34:7095–7110.
- Deleu, T., Góis, A., Emezue, C., Rankawat, M., Lacoste-Julien, S., Bauer, S., and Bengio, Y. (2022). Bayesian structure learning with generative flow networks. In *Uncertainty in Artificial Intelligence*, pages 518–528. PMLR.

- Diamond, S. and Boyd, S. (2016). Cvxpy: A python-embedded modeling language for convex optimization. *Journal of Machine Learning Research*, 17(83):1–5.
- Dixit, A., Parnas, O., Li, B., Chen, J., Fulco, C. P., Jerby-Arnon, L., Marjanovic, N. D., Dionne, D., Burks, T., Raychowdhury, R., Adamson, B., Norman, T. M., Lander, E. S., Weissman, J. S., Friedman, N., and Regev, A. (2016). Perturb-Seq: Dissecting Molecular Circuits with Scalable Single-Cell RNA Profiling of Pooled Genetic Screens. *Cell*, 167(7):1853–1866.e17. Publisher: Cell Press.
- Feng, C., Peets, E. M., Zhou, Y., Crepaldi, L., Usluer, S., Dunham, A., Braunger, J. M., Su, J., Strauss, M. E., Muraro, D., Cheam, K. A. X., Bonder, M. J., Nogales, E. G., Cooper, S., Bassett, A., Leonard, S., Gu, Y., Fusing, B., Burke, D., Parts, L., Stegle, O., and Velten, B. (2024). A genome-scale single cell CRISPRi map of trans gene regulation across human pluripotent stem cell lines. Pages: 2024.11.28.625833 Section: New Results.
- Friedman, N. and Koller, D. (2003). Being Bayesian About Network Structure. A Bayesian Approach to Structure Discovery in Bayesian Networks. *Machine Learning*, 50(1):95–125.
- Gasperini, M., Hill, A. J., McFaline-Figueroa, J. L., Martin, B., Kim, S., Zhang, M. D., Jackson, D., Leith, A., Schreiber, J., Noble, W. S., Trapnell, C., Ahituv, N., and Shendure, J. (2019). A Genome-wide Framework for Mapping Gene Regulation via Cellular Genetic Screens. *Cell*, 176(1-2):377–390.e19. Publisher: Cell Press.
- Geiger, D. and Heckerman, D. (2002). Parameter priors for directed acyclic graphical models and the characterization of several probability distributions. *The Annals of Statistics*, 30(5):1412–1440. Publisher: Institute of Mathematical Statistics.
- Hägele, A., Rothfuss, J., Lorch, L., Somnath, V. R., Schölkopf, B., and Krause, A. (2023). Bacadi: Bayesian causal discovery with unknown interventions. In *International Conference on Artificial Intelligence and Statistics*, pages 1411–1436. PMLR.
- Hauser, A. and Bühlmann, P. (2012). Characterization and greedy learning of interventional markov equivalence classes of directed acyclic graphs. *The Journal of Machine Learning Research*, 13(1):2409–2464.
- Hoffman, M. D., Gelman, A., et al. (2014). The no-u-turn sampler: adaptively setting path lengths in hamiltonian monte carlo. *J. Mach. Learn. Res.*, 15(1):1593–1623.
- Hyttinen, A., Eberhardt, F., and Hoyer, P. O. (2012). Learning Linear Cyclic Causal Models with Latent Variables. *Journal of Machine Learning Research*, 13(109):3387–3439.
- Imbens, G. W. (2014). Instrumental Variables: An Econometrician’s Perspective. *Statistical Science*, 29(3):323–358. Publisher: Institute of Mathematical Statistics.
- Levis, A. W., Kennedy, E. H., and Keele, L. (2024). Nonparametric identification and efficient estimation of causal effects with instrumental variables. arXiv:2402.09332 [stat].
- Liu, Q. and Ihler, A. (2011). Learning scale free networks by reweighted ℓ_1 regularization. In Gordon, G., Dunson, D., and Dudík, M., editors, *Proceedings of the Fourteenth International Conference on Artificial Intelligence and Statistics*, volume 15 of *Proceedings of Machine Learning Research*, pages 40–48, Fort Lauderdale, FL, USA. PMLR.
- Liu, X., Li, Y. I., and Pritchard, J. K. (2019). Trans Effects on Gene Expression Can Drive Omnigenic Inheritance. *Cell*, 177(4):1022–1034.e6. Publisher: Elsevier Inc.
- Lopez, R., Hütter, J.-C., Pritchard, J., and Regev, A. (2022). Large-scale differentiable causal discovery of factor graphs. *Advances in Neural Information Processing Systems*, 35:19290–19303.
- Lorch, L., Rothfuss, J., Schölkopf, B., and Krause, A. (2021). Dibs: Differentiable bayesian structure learning. *Advances in Neural Information Processing Systems*, 34:24111–24123.
- Madigan, D., York, J., and Allard, D. (1995). Bayesian graphical models for discrete data. *International statistical review/revue internationale de statistique*, pages 215–232.

- Montalbano, A., Canver, M. C., and Sanjana, N. E. (2017). High-Throughput Approaches to Pinpoint Function within the Noncoding Genome. *Molecular Cell*, 68(1):44–59. Publisher: Cell Press.
- Nazaret, A., Hong, J., Azizi, E., and Blei, D. (2023). Stable differentiable causal discovery. *arXiv preprint arXiv:2311.10263*.
- Neal, R. M. (2003). Slice sampling. *The annals of statistics*, 31(3):705–767.
- Papaspiliopoulos, O., Roberts, G. O., and Sköld, M. (2007). A general framework for the parametrization of hierarchical models. *Statistical Science*, pages 59–73.
- Pasaniuc, B. and Price, A. L. (2017). Dissecting the genetics of complex traits using summary association statistics. *Nature Reviews Genetics*, 18(2):117–127. Publisher: Nature Publishing Group.
- Pearl, J. (2000). *Causality : models, reasoning, and inference*. Cambridge, U.K. ; New York : Cambridge University Press.
- Pearl, J. (2009). *Causality*. Cambridge university press.
- Phan, D., Pradhan, N., and Jankowiak, M. (2019). Composable effects for flexible and accelerated probabilistic programming in numpyro. *arXiv preprint arXiv:1912.11554*.
- Replogle, J. M., Saunders, R. A., Pogson, A. N., Hussmann, J. A., Lenail, A., Guna, A., Mascibroda, L., Wagner, E. J., Adelman, K., Lithwick-Yanai, G., Iremadze, N., Oberstrass, F., Lipson, D., Bonnar, J. L., Jost, M., Norman, T. M., and Weissman, J. S. (2022). Mapping information-rich genotype-phenotype landscapes with genome-scale Perturb-seq. *Cell*, 185(14):2559–2575.e28. Publisher: Elsevier BV.
- Sani, N., Lee, J., and Shpitser, I. (2020). Identification and Estimation of Causal Effects Defined by Shift Interventions. In *Proceedings of the 36th Conference on Uncertainty in Artificial Intelligence (UAI)*, pages 949–958. PMLR. ISSN: 2640-3498.
- Shimizu, S., Hoyer, P. O., Hyvärinen, A., Kerminen, A., and Jordan, M. (2006). A linear non-gaussian acyclic model for causal discovery. *Journal of Machine Learning Research*, 7(10).
- Stephens, M. (2017). False discovery rates: a new deal. *Biostatistics*, 18(2):275–294.
- Tian, J. and He, R. (2009). Computing posterior probabilities of structural features in Bayesian networks. In *Proceedings of the Twenty-Fifth Conference on Uncertainty in Artificial Intelligence*, UAI '09, pages 538–547, Arlington, Virginia, USA. AUAI Press.
- Toth, C., Knoll, C., Pernkopf, F., and Peharz, R. (2024). Effective bayesian causal inference via structural marginalisation and autoregressive orders. *arXiv preprint arXiv:2402.14781*.
- Toth, C., Lorch, L., Knoll, C., Krause, A., Pernkopf, F., Peharz, R., and Von Kügelgen, J. (2022). Active bayesian causal inference. *Advances in Neural Information Processing Systems*, 35:16261–16275.
- Verma, T. and Pearl, J. (1990). Equivalence and Synthesis of Causal Models. In *Proceedings of the Sixth Conference Annual Conference on Uncertainty in Artificial Intelligence (UAI-90)*, pages 220–227.
- Vonk, M. C., Malekovic, N., Bäck, T., and Kononova, A. V. (2023). Disentangling causality: assumptions in causal discovery and inference. *Artificial Intelligence Review*, 56(9):10613–10649.
- Weinstock, J. S., Arce, M. M., Freimer, J. W., Ota, M., Marson, A., Battle, A., and Pritchard, J. K. (2024). Gene regulatory network inference from CRISPR perturbations in primary CD4+ T cells elucidates the genomic basis of immune disease. *Cell Genomics*, 4(11). Publisher: Elsevier.
- Wray, N. R., Wijmenga, C., Sullivan, P. F., Yang, J., and Visscher, P. M. (2018). Common Disease Is More Complex Than Implied by the Core Gene Omnigenic Model. *Cell*, 173(7):1573–1580. Publisher: Elsevier Inc.
- Xue, A., Rao, J., Sankararaman, S., and Pimentel, H. (2023). dotears: Scalable, consistent DAG estimation using observational and interventional data. arXiv: 2305.19215.

- Yang, K. D., Katcoff, A., and Uhler, C. (2018). Characterizing and Learning Equivalence Classes of Causal DAGs under Interventions. *35th International Conference on Machine Learning, ICML 2018*, 12:8823–8839. arXiv: 1802.06310 Publisher: International Machine Learning Society (IMLS) ISBN: 9781510867963.
- Zhang, L., Carpenter, B., Gelman, A., and Vehtari, A. (2022). Pathfinder: Parallel quasi-newton variational inference. *Journal of Machine Learning Research*, 23(306):1–49.
- Zheng, X., Aragam, B., Ravikumar, P. K., and Xing, E. P. (2018). Dags with no tears: Continuous optimization for structure learning. *Advances in neural information processing systems*, 31.

A Covariance structure of total causal effect estimates

Our goal is to estimate the covariance between the total causal effect estimates, given by

$$\text{Cov}(\hat{R}_{ij}, \hat{R}_{kl}) = \mathbb{E}[(\hat{R}_{ij} - \mathbb{E}[\hat{R}_{ij}])(\hat{R}_{kl} - \mathbb{E}[\hat{R}_{kl}])] \quad (14)$$

We assume the estimator takes a two-stage linear form, such that the function linking the instruments to the exposure and the exposure to the outcome are both linear:

$$\hat{y}_i = P_i y_i, \quad (15)$$

$$\hat{y}_j = \hat{R}_{ij} y_i, \quad (16)$$

$$\hat{R}_{ij} = \hat{Q}_i y_j, \quad (17)$$

where we have written P_i as the projection matrix onto the instruments for i , and \hat{Q}_i as the regression operator that determines the coefficients from \hat{y}_i . For example, in generalized least squares we would write $P_i = X_i(X_i^\top W_i X_i)^{-1} X_i^\top W_i$ and $\hat{Q}_i = (\hat{y}_i^\top W_y \hat{y}_i)^{-1} \hat{y}_i^\top W_y$ for weight matrices W_i and W_y . We assume the estimators are unbiased so that $\forall i, j, \mathbb{E}[\hat{R}_{ij}] = R_{ij}$.

Using 7, we can write y_j as

$$y_j = X\beta R_{:j} + \epsilon R_{:j}, \quad (18)$$

where $R_{:j}$ refers to the j 'th column of R . Using this, we can write

$$\hat{R}_{ij} = \hat{Q}_i(X\beta R_{:j} + \epsilon R_{:j}). \quad (19)$$

Similarly, writing y_i as $y_i R_{ij} = X\beta R_{:i} R_{ij} + \epsilon R_{:i} R_{ij}$ and adding and subtracting $\hat{Q}_i y_i$ to 19 and collecting terms we have,

$$\hat{R}_{ij} = \hat{Q}_i(X\beta R_{:j} + \epsilon R_{:j}) + \hat{Q}_i y_i R_{ij} - \hat{Q}_i y_i R_{ij} \quad (20)$$

$$= \hat{Q}_i(y_i R_{ij} + X\beta R_{:j} - X\beta R_{:i} R_{ij} + \epsilon R_{:j} - \epsilon R_{:i} R_{ij}) \quad (21)$$

$$= R_{ij} + \hat{Q}_i(X\beta R_{:j} - X\beta R_{:i} R_{ij} + \epsilon R_{:j} - \epsilon R_{:i} R_{ij}). \quad (22)$$

Because \hat{Q}_i projects onto instruments for y_i , all effects $X\beta R_{:j}$ must travel through y_i , so $\hat{Q}_i X\beta R_{:j} = \hat{Q}_i X\beta R_{:i} R_{ij}$. This leaves us with,

$$\hat{R}_{ij} - R_{ij} = \hat{Q}_i(\epsilon R_{:j} - \epsilon R_{:i} R_{ij}) \quad (23)$$

$$= \hat{Q}_i(y_j - R_{ij} y_i) \quad (24)$$

$$= \hat{Q}_i \epsilon_{ij}. \quad (25)$$

Using this and independence across samples we see that the covariance entries are given by

$$\text{Cov}(\hat{R}_{ij}, \hat{R}_{kl}) = \mathbb{E}[\hat{Q}_i \epsilon_{ij} \epsilon_{kl}^\top \hat{Q}_k^\top] \quad (26)$$

$$= \hat{Q}_i \hat{Q}_k^\top \text{Cov}(\epsilon_{ij}, \epsilon_{kl}). \quad (27)$$

In the least squares case this leads to the plug in estimator 8,

$$\hat{S}_{ijkl} = \frac{\text{Cov}(\hat{y}_i, \hat{y}_k) \text{Cov}(\hat{\epsilon}_{ij}, \hat{\epsilon}_{kl})}{n \text{Var}(\hat{y}_i) \text{Var}(\hat{y}_k)}.$$

B Prior estimation

B.1 ER global sparsity prior estimation

As described in Section 3.2, we place a flexible empirical Bayes prior on each direct effect G_{ij} . Formally, the prior is

$$p(G_{ij} \mid \{\pi_k\}, \{\sigma_k^2\}, \hat{s}_{ij}) \propto \pi_0 \mathcal{N}(0, \sigma_0^2 + \hat{s}_{ij}^2) + \sum_{k=1}^K \pi_k \mathcal{N}(0, \sigma_k^2 + \hat{s}_{ij}^2), \quad (28)$$

where π_0 corresponds to a near-zero "spike" component and the slab weights $\{\pi_k\}$ are learned over a grid of variances $\{\sigma_k^2\}$. The standard error of the estimate of \hat{R}_{ij} , given by $\hat{s}_{ij} = \hat{S}_{ijij}$, accounts for edge specific heteroskedasticity. We fit the parameters $\{\pi_k\}$ to the observed \hat{R} using Expectation Maximization (EM).

The goal of the global sparsity prior is to estimate a flexible, data-driven mixture prior over all off-diagonal entries of the total effect matrix \hat{R} , capturing both sparsity and a range of plausible effect sizes. We require the following constraints:

$$\pi_0 + \sum_{k=1}^K \pi_k = 1, \quad \pi_0 \geq 0, \quad \pi_k \geq 0. \quad (29)$$

To estimate the mixture weights $\{\pi_0, \pi_1, \dots, \pi_K\}$, we maximize a penalized likelihood over the observed $\{w_i\}_{i=1}^N$. The log-likelihood of the data under this model is:

$$\log L(\pi_0, \pi_1, \dots, \pi_K) = \sum_{i=1}^N \log \left[\pi_0 f_0(w_i) + \sum_{k=1}^K \pi_k f_k(w_i) \right], \quad (30)$$

where $f_0(w_i) = \mathcal{N}(w_i; 0, \sigma_0^2 + \hat{s}_i^2)$ and $f_k(w_i) = \mathcal{N}(w_i; 0, \sigma_k^2 + \hat{s}_i^2)$ incorporate edge specific standard errors \hat{s}_i from IV regression to reflect heteroskedasticity across edges. We add a Dirichlet-like penalty to the slab components to encourage sparsity:

$$\text{Obj}(\pi_0, \pi_1, \dots, \pi_K) = \sum_{i=1}^N \log \left[\pi_0 f_0(w_i) + \sum_{k=1}^K \pi_k f_k(w_i) \right] + (\alpha - 1) \sum_{k=1}^K \log \pi_k, \quad (31)$$

where $\alpha = 2$ by default. A larger α concentrates more mass on the spike by shrinking the slab weights. We optimize this penalized objective using the EM algorithm. In the E-step, for each w_i , we compute the posterior responsibility for each mixture component:

$$z_{i,0} = \frac{\pi_0 f_0(w_i)}{\pi_0 f_0(w_i) + \sum_{m=1}^K \pi_m f_m(w_i)}, \quad (32)$$

$$z_{i,k} = \frac{\pi_k f_k(w_i)}{\pi_0 f_0(w_i) + \sum_{m=1}^K \pi_m f_m(w_i)}. \quad (33)$$

We then compute expected counts:

$$n_0 = \sum_{i=1}^N z_{i,0}, \quad n_k = \sum_{i=1}^N z_{i,k}, \quad k = 1, \dots, K. \quad (34)$$

In the M-step, we update the mixture weights by maximizing the complete-data penalized log-likelihood:

$$\pi_0 = \frac{n_0}{N + (\alpha - 1)K}, \quad (35)$$

$$\pi_k = \frac{n_k + (\alpha - 1)}{N + (\alpha - 1)K}, \quad k = 1, \dots, K. \quad (36)$$

These updates ensure that the weights remain normalized and non-negative.

B.2 Localizing ER and SF global sparsity prior estimation

To localize the global prior, we calculate the covariance $\Sigma = \text{Cov}(Y_C)$ where Y_C are the non-intervened control samples. We then normalize this into a matrix of interaction strengths $\xi := \frac{\Sigma \odot \Sigma}{\|\Sigma \odot \Sigma\|_F^2}$ such that each $\xi_{ij} \in [0, 1]$.

We use this to construct edge specific weights π_k^{ij} by solving the convex quadratic program,

$$\min_{\pi_0, \pi_k} \sum_{i \neq j} \left[\left(\pi_k^{i,j} - \xi_{ij} \right)^2 + \left(\pi_0^{i,j} - (1 - \xi_{ij}) \right)^2 \right], \quad (37)$$

subject to the constraints,

$$\pi_0^{i,j} + \pi_k^{i,j} = 1 \quad \forall i \neq j, \quad (38)$$

$$\pi_0^{i,i} = 1, \quad \pi_k^{i,i} = 0 \quad \forall i, \quad (39)$$

$$\pi_0^{i,j} \geq 0, \quad \pi_k^{i,j} \geq 0 \quad \forall i, j, \quad (40)$$

with the sparsity constraint depending on the prior:

$$\text{ER: } \sum_{i \neq j} \pi_0^{i,j} = \pi_0^{\text{global}} \cdot (D^2 - D), \tag{41}$$

$$\text{SF: } \sum_{j > i} \pi_{0,ij} = \pi_{0,i}(D - i - 1) \quad \forall i, \tag{42}$$

where π_0^{global} is the average sparsity level estimated from the EM step from ER, and $\pi_{0,i} \in [0, 1]$ reflects the empirical sparsity of node i from SF. We solve this convex optimization problem using the CVXPY package (Diamond and Boyd, 2016).

C Inference hyperparameters

We used No-U-Turn Sampler (NUTS), with a target acceptance probability of 0.7, which balances step size and acceptance rate in Hamiltonian Monte Carlo, and a maximum tree depth of 10 to ensure thorough posterior exploration without excessive computation. The sampler is initialized at the median of three prior predictive draws, providing a stable starting point for sampling. We ran three chains with 300 warm-up steps and 1000 samples per chain.

D Experiment details

D.1 Synthetic data generation and processing

To evaluate performance across varied causal regimes, we used the simulator from (Brown et al., 2023). We generated synthetic datasets with a known intervention design matrix from the model 7 using both Erdős-Rényi (ER) and scale-free (SF) graph topologies while varying the graph size, $D \in \{50, 150, 250, 500\}$. To keep sparsity comparable across sizes, we targeted an average node degree of approximately 5. For ER, we set the edge inclusion probability to $p \approx 5/D$, specifically $p = \{0.10, 0.033, 0.02, 0.01\}$ for $D = \{50, 150, 250, 500\}$. For SF, we empirically calibrated p per D to achieve an average degree of 5, selecting $p = \{0.066, 0.108, 0.124, 0.139\}$ for $D = \{50, 150, 250, 500\}$ via repeated simulation. Edge weights were drawn from a PERT distribution (Clark, 1962) with minimum $v/2$, mode v , and maximum $2v$, where v controls the typical magnitude of causal effects on a per-variance scale, and we set $v = 0.25$. All data were normalized to mean 0, variance 1 in the control samples. To specify the strength of interventions, we defined the effect size β as the number of standard deviations by which the mean of Y_i shifts when the intervention $X_i = 1$ is applied. The intervention strength was fixed at $\beta = -2$. Each configuration included $D \times 100$ interventional samples and $D \times 100$ control samples ($2D \times 100$ total). Additionally, for $D = 50$ we created datasets with varying intervention sample sizes, $N \in \{5, 15, 25, 50, 75, 100\}$, under the same design. For baselines that operate on observational data only (GES, NOTEARS, LiNGAM, BayesDAG), we generated purely observational datasets with $2D \times 100$ control samples ($N = 0$) so that the total sample size matches the interventional datasets. For ablations we set $\beta = -1.5$ and $v = 0.2$ and used the same graph construction with ER graphs at $D \in \{50, 150, 250, 500\}$ and SF graphs only at $D = 50$ with 100 intervention samples per variable and $D \times 100$ control samples. All configurations were replicated across ten replicates to assess robustness of the methods.

D.2 K562 Perturb-seq Data and processing

For real data, we analyzed both the genome-wide (GWPS) and essential Perturb-seq screens in K562 cells (Replogle et al., 2022). We considered genes present in both panels and retained genes where the estimated per-variance effect-size of the intervention on the target gene was at least -0.75 standard deviations, and where there were at least 50 cells receiving a guide targeting that gene. This yielded 521 well-captured genes for downstream analysis. Raw single-cell matrices were obtained from Figshare (<https://plus.figshare.com/ndownloader/files/35773075>) to regress out cell-cycle effects prior to downstream inference. This dataset contains CRISPR-inhibition guide RNA targeting each of 2,057 essential genes in the essential panel, and targeting approximately 9,866 expressed genes in the GWPS panels, with each cell receiving one guide targeting one gene.

To enhance the perturbation signal and reduce cell cycle confounding, we regress out per-cell S and G2M module scores prior to inference. Let $Y \in \mathbb{R}^{C \times G}$ denote the log-normalized expression matrix after size-factor

normalization, where c indexes cells and g indexes genes. Let s_c be the S phase module score and m_c the G2M module score, computed per cell from standard S and G2M gene sets with expression matched control genes. For each gene g , we fit

$$Y_{cg} = \alpha_g + \beta_g^{(S)} s_c + \beta_g^{(G2M)} m_c + \varepsilon_{cg}.$$

We define residuals using the fitted coefficients, $\hat{\varepsilon}_{cg} = Y_{cg} - \hat{\alpha}_g - \hat{\beta}_g^{(S)} s_c - \hat{\beta}_g^{(G2M)} m_c$. Within each 10x GEM group h , we compute μ_{gh}^{NTC} and σ_{gh}^{NTC} as the mean and standard deviation of $\hat{\varepsilon}_{cgh}$ over non-targeting control (NTC) cells in group h and standardize residuals per gene using these NTC statistics within each group, $Z_{cgh} = \frac{\hat{\varepsilon}_{cgh} - \mu_{gh}^{\text{NTC}}}{\sigma_{gh}^{\text{NTC}}}$. Here Z_{cgh} denotes the standardized residual for cell c , gene g , and GEM group h . This yields a cell-cycle-adjusted and GEM-normalized matrix Z for downstream analysis. We used two-stage least squares to estimate causal effects using guide presence as an instrumental variable. Note that because each cell receives one guide, there is no covariance between \hat{y}_i and \hat{y}_k when $i \neq k$. Thus, the covariance [8](#) simplifies to

$$\hat{S}_{ijkl} = \begin{cases} \frac{1}{n\hat{\beta}_i^2} \text{Cov}(\hat{\varepsilon}_{ij}, \hat{\varepsilon}_{il}) & \text{if } i = k, \\ 0 & \text{otherwise.} \end{cases}$$

For each gene, we estimated the effect size $\hat{\beta}_i$ of the instrument on its target gene using linear regression of gene expression on perturbation status. We then restricted analyses to the 521 genes shared by the GWPS and essential panels.

D.3 Baselines

To evaluate our method in a wider context, we compare our model (IBCD) to a diverse set of different methods. We describe our baselines briefly in the following.

- **inspre** ([Brown et al., 2023](#)) inverse sparse regression (inspre) learns a sparse left inverse of the average causal effect matrix from per target interventions and reconstructs a weighted causal network. We use the implementation at <https://github.com/brielin/inspre> with default hyperparameters and set DAG=TRUE to enforce acyclicity.
- **LiNGAM** ([Shimizu et al., 2006](#)) LiNGAM assumes linear relations, acyclicity, and independent non-Gaussian noise to recover a causal ordering and estimates edge weights by regression. We used the implementations from the `pcaIlg` R package with default parameter settings.
- **GES** ([Chickering, 2002](#)) Greedy Equivalence Search (GES) is a greedy score-based method for causal discovery using the BIC score. We used the implementations from the `pcaIlg` R package with default parameter settings.
- **GIES** ([Hauser and Bühlmann, 2012](#)) Greedy Interventional Equivalence Search (GIES) is an interventional extension of GES ([Chickering, 2002](#)) that uses known intervention targets to score structures and orient edges. We used the implementations from the `pcaIlg` R with default settings. We include GIES to highlight the benefit of interventional data, and in our experiments it recovered graph structure better than the observational-only GES.
- **SDCD** ([Nazaret et al., 2023](#)) Stable Differentiable Causal Discovery (SDCD) is a differentiable, score based method that enforces acyclicity with a spectral radius penalty and trains in two stages, edge preselection then penalized differentiable causal discovery, to improve stability and scale. We use the implementation at <https://github.com/azizilab/sdcd> with default parameters, setting `thresholding=True` to enable the built-in, data-adaptive thresholding driven by inferred effect sizes, following the jupyter notebook tutorial.
- **NOTEARS** ([Zheng et al., 2018](#)) NOTEARS reformulates score-based DAG learning as a smooth equality-constrained optimization using a matrix-exponential acyclicity function, enabling global continuous search with standard solvers. We use the implementation at <https://github.com/xunzheng/notears> and set `w_threshold=0` to apply thresholding uniformly in post-processing. Our simulations use unit-normalized data such that edge weights represent per-variance effect sizes; therefore the default threshold 0.3 is well above the median simulated effect size and would degrade performance.

- **BayesDAG** (Annadani et al., 2023) BayesDAG combines hybrid strategy where MCMC learns permutations and mechanism parameters, while variational inference infers DAG edges given the learned permutations. We use the implementation at <https://github.com/microsoft/Project-BayesDAG> with default settings.
- **LLCB** (Weinstock et al., 2024) Linear Latent Causal Bayes (LLCB) is a Bayesian extension of Linear Latent Causal model (Hyttinen et al., 2012) that deconvolves total perturbation effects into direct gene–gene edges using sparsity and spectral-radius priors using a variational method, Pathfinder (Zhang et al., 2022). We use the implementation at <https://github.com/weinstockj/LLCB> with default settings.

E Oracle priors from the true graph

In our ablation studies the oracle prior uses the true matrix G to directly set the spike probability and serves as an upper bound that isolates the impact of learning priors from observational summaries. We flatten the off diagonal entries of G into $w = (w_1, \dots, w_N)$ with $N = D(D - 1)$. We compute

$$\pi_0 = \frac{1}{N} \sum_{i=1}^N \mathbb{1}\{w_i = 0\}.$$

The slab mass is $1 - \pi_0$. These weights parameterize the spike and slab horseshoe prior over G used in the ablation studies.

F Supplementary figures and tables

Dim	metric	50D	150D	250D	500D
ER baseline	F1	0.875 ± 0.023	0.848 ± 0.019	0.858 ± 0.011	0.877 ± 0.015
	SHD	58.9 ± 8.34	216.8 ± 25.36	335.9 ± 25.86	560.0 ± 56.47
ER with SF prior	F1	0.908 ± 0.017	0.836 ± 0.022	0.789 ± 0.035	0.576 ± 0.131
	SHD	44.5 ± 8.34	255.8 ± 33.19	598.0 ± 120.70	3160.8 ± 1502.28

Table 3: Ablation study comparing the mean and standard deviation of F1 and SHD metrics between the ER baseline and ER with SF prior across different graph dimensions, averaged over ten replicates.

Dim	Graph	IBCD	inspre	GIES	GES	LiNGAM	SDCD	NOTEARS	BayesDAG	LLCB
50D	ER	0.971 ± 0.008	0.921 ± 0.018	0.536 ± 0.129	0.329 ± 0.054	0.344 ± 0.058	0.422 ± 0.102	0.559 ± 0.046	0.400 ± 0.040	0.408 ± 0.037
	SF	0.965 ± 0.011	0.886 ± 0.020	0.617 ± 0.074	0.451 ± 0.042	0.801 ± 0.107	0.642 ± 0.065	0.474 ± 0.050	0.483 ± 0.086	0.426 ± 0.077
150D	ER	0.978 ± 0.004	0.893 ± 0.008	0.638 ± 0.119	0.385 ± 0.066	0.285 ± 0.022	0.300 ± 0.040	0.801 ± 0.027	NA	NA
	SF	0.959 ± 0.009	0.808 ± 0.011	0.520 ± 0.059	0.447 ± 0.027	0.841 ± 0.072	0.582 ± 0.042	0.537 ± 0.029	NA	NA
250D	ER	0.979 ± 0.003	0.879 ± 0.006	0.710 ± 0.140	0.443 ± 0.063	0.276 ± 0.026	0.311 ± 0.029	0.857 ± 0.010	NA	NA
	SF	0.963 ± 0.004	0.785 ± 0.011	0.492 ± 0.033	0.441 ± 0.028	0.836 ± 0.040	0.597 ± 0.036	0.551 ± 0.028	NA	NA
500D	ER	0.982 ± 0.003	0.851 ± 0.010	0.789 ± 0.110	0.590 ± 0.076	0.280 ± 0.031	0.307 ± 0.016	NA	NA	NA
	SF	0.943 ± 0.015	0.738 ± 0.010	0.447 ± 0.025	0.437 ± 0.027	0.856 ± 0.029	0.659 ± 0.019	NA	NA	NA

Table 4: Comparison of mean and standard deviation of F1 with increasing numbers of dimensions on ER and SF graphs in Figure 2. NA values correspond to failed runs, typically due to a 12 h timeout or termination for exceeding resource limits as noted in Table 2.

Dim	Graph	IBCD	inspre	GIES	GES	LiNGAM	SDCD	NOTEARS	BayesDAG	LLCB
50D	ER	14.8 ± 4.26	41.3 ± 11.09	374.6 ± 168.58	632.1 ± 106.99	510.8 ± 82.95	219.9 ± 44.66	184.3 ± 24.53	391.7 ± 19.52	640.8 ± 114.74
	SF	16.6 ± 5.76	56.0 ± 12.87	218.0 ± 62.85	329.0 ± 49.67	101.9 ± 55.63	137.2 ± 30.98	196.6 ± 32.09	287.4 ± 58.90	316.4 ± 41.47
150D	ER	32.0 ± 6.99	163.4 ± 15.15	829.7 ± 375.50	1958.8 ± 472.12	1889.4 ± 145.69	695.0 ± 40.04	266.3 ± 34.63	NA	NA
	SF	61.2 ± 13.65	279.7 ± 24.39	1024.9 ± 214.49	1247.2 ± 143.42	261.6 ± 143.87	462.8 ± 57.69	543.9 ± 53.11	NA	NA
250D	ER	53.5 ± 8.58	308.9 ± 23.67	1094.3 ± 762.81	2819.5 ± 739.89	3254.1 ± 317.28	1178.5 ± 58.18	329.0 ± 20.62	NA	NA
	SF	91.7 ± 10.80	512.0 ± 43.91	1927.5 ± 261.34	2247.6 ± 328.42	435.5 ± 118.99	731.6 ± 85.21	862.1 ± 90.74	NA	NA
500D	ER	91.5 ± 12.79	707.9 ± 28.25	1417.9 ± 1009.78	3348.2 ± 980.04	6306.1 ± 704.84	2638.6 ± 83.47	NA	NA	NA
	SF	284.8 ± 74.40	1316.5 ± 37.60	4831.8 ± 434.00	4972.1 ± 536.01	782.1 ± 190.47	1319.3 ± 88.99	NA	NA	NA

Table 5: Comparison of mean and standard deviation of SHD with increasing numbers of dimensions on ER and SF graphs in Figure 2. NA values correspond to failed runs, typically due to a 12 h timeout or termination for exceeding resource limits as noted in Table 2.

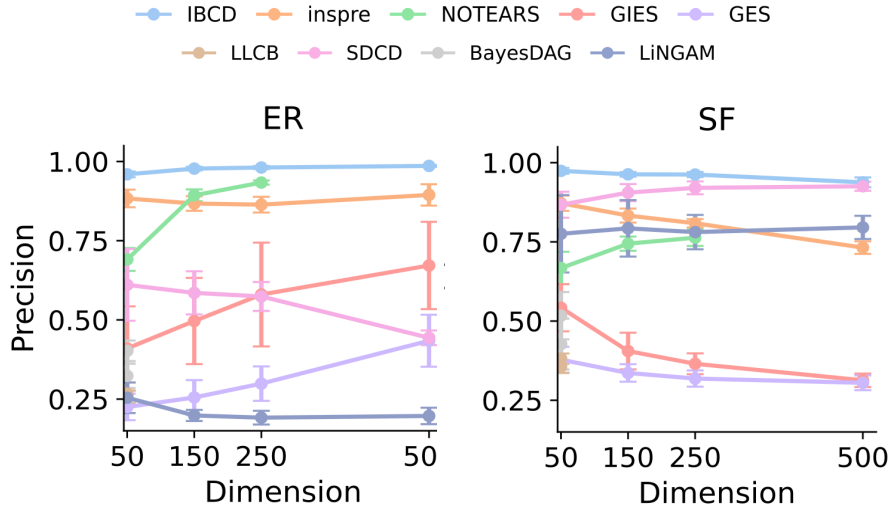


Figure 7: Comparison of precision with increasing numbers of dimensions on ER and SF graphs, using 100 intervention samples per variable.

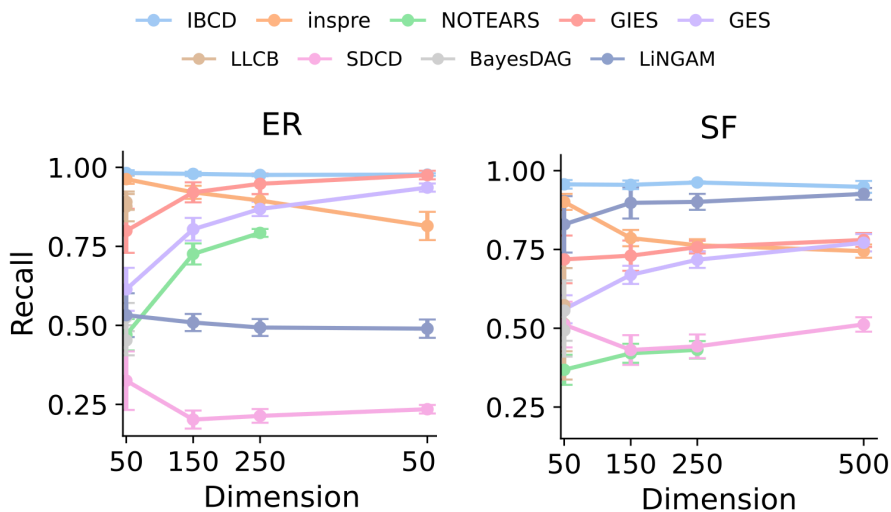


Figure 8: Comparison of recall with increasing numbers of dimensions on ER and SF graphs, using 100 intervention samples per variable.

Sample	Graph	IBCD	inspre	GIES	GES	LiNGAM	SDCD	NOTEARS	BayesDAG	LLCB
5	ER	0.431 ± 0.030	0.311 ± 0.030	0.642 ± 0.077	0.434 ± 0.071	0.299 ± 0.054	0.737 ± 0.036	0.499 ± 0.055	0.007 ± 0.009	0.847 ± 0.023
	SF	0.518 ± 0.054	0.279 ± 0.037	0.536 ± 0.036	0.452 ± 0.049	0.522 ± 0.078	0.622 ± 0.065	0.443 ± 0.049	0.002 ± 0.004	0.633 ± 0.043
15	ER	0.708 ± 0.035	0.517 ± 0.029	0.622 ± 0.075	0.394 ± 0.079	0.364 ± 0.054	0.684 ± 0.059	0.535 ± 0.058	0.220 ± 0.058	0.872 ± 0.026
	SF	0.784 ± 0.019	0.496 ± 0.035	0.592 ± 0.072	0.498 ± 0.044	0.760 ± 0.092	0.737 ± 0.051	0.471 ± 0.045	0.227 ± 0.070	0.586 ± 0.128
25	ER	0.813 ± 0.026	0.630 ± 0.024	0.609 ± 0.137	0.387 ± 0.053	0.332 ± 0.061	0.628 ± 0.059	0.542 ± 0.057	0.355 ± 0.048	0.882 ± 0.025
	SF	0.868 ± 0.022	0.589 ± 0.032	0.640 ± 0.049	0.476 ± 0.078	0.789 ± 0.077	0.740 ± 0.046	0.462 ± 0.050	0.390 ± 0.070	0.564 ± 0.161
50	ER	0.913 ± 0.014	0.779 ± 0.018	0.553 ± 0.116	0.334 ± 0.042	0.356 ± 0.041	0.513 ± 0.085	0.549 ± 0.052	0.426 ± 0.037	0.891 ± 0.025
	SF	0.934 ± 0.011	0.749 ± 0.013	0.647 ± 0.067	0.469 ± 0.060	0.786 ± 0.083	0.703 ± 0.048	0.458 ± 0.054	0.504 ± 0.078	0.573 ± 0.146
75	ER	0.950 ± 0.018	0.867 ± 0.023	0.534 ± 0.135	0.344 ± 0.053	0.338 ± 0.057	0.461 ± 0.119	0.563 ± 0.063	0.433 ± 0.049	0.878 ± 0.043
	SF	0.953 ± 0.013	0.827 ± 0.027	0.649 ± 0.036	0.481 ± 0.050	0.828 ± 0.072	0.694 ± 0.051	0.476 ± 0.062	0.538 ± 0.051	0.532 ± 0.166
100	ER	0.971 ± 0.008	0.921 ± 0.018	0.536 ± 0.129	0.329 ± 0.054	0.344 ± 0.058	0.422 ± 0.102	0.559 ± 0.046	0.400 ± 0.040	0.876 ± 0.047
	SF	0.965 ± 0.011	0.886 ± 0.020	0.617 ± 0.074	0.451 ± 0.042	0.801 ± 0.107	0.642 ± 0.065	0.474 ± 0.050	0.483 ± 0.086	0.514 ± 0.177

Table 6: Comparison of mean and standard deviation of F1 with increasing numbers of intervention sample sizes on ER and SF graphs with $D = 50$ in Figure 3.

Sample	Graph	IBCD	inspre	GIES	GES	LiNGAM	SDCD	NOTEARS	BayesDAG	LLCB
5	ER	225.3 ± 22.72	480.7 ± 71.30	203.5 ± 55.72	348.4 ± 62.84	304.6 ± 36.67	128.5 ± 21.66	208.7 ± 30.08	248.7 ± 16.57	1024.6 ± 48.99
	SF	186.9 ± 23.59	423.0 ± 85.45	225.3 ± 34.65	268.3 ± 36.97	183.5 ± 36.10	167.9 ± 34.80	206.8 ± 31.47	241.2 ± 27.53	891.3 ± 23.32
15	ER	135.8 ± 19.32	280.3 ± 28.10	243.2 ± 77.52	452.8 ± 103.42	452.0 ± 73.57	141.5 ± 29.49	194.6 ± 29.35	253.9 ± 21.92	759.6 ± 89.35
	SF	96.3 ± 14.67	244.7 ± 43.44	214.3 ± 58.74	269.1 ± 43.67	116.1 ± 48.42	110.9 ± 25.36	198.6 ± 29.78	230.8 ± 29.37	483.9 ± 81.67
25	ER	93.3 ± 16.42	225.2 ± 19.60	271.2 ± 136.74	484.6 ± 81.31	514.0 ± 85.27	155.3 ± 27.92	191.3 ± 30.22	261.1 ± 23.30	702.8 ± 92.57
	SF	59.3 ± 7.59	212.7 ± 29.58	190.4 ± 42.08	289.1 ± 67.28	103.3 ± 37.02	108.8 ± 25.94	202.0 ± 33.13	223.6 ± 37.25	389.2 ± 76.47
50	ER	44.2 ± 8.28	126.0 ± 17.38	338.0 ± 132.32	595.6 ± 85.51	500.3 ± 71.75	192.6 ± 35.68	188.6 ± 27.82	303.5 ± 30.78	672.2 ± 87.79
	SF	30.5 ± 4.25	126.8 ± 16.64	193.5 ± 58.40	302.6 ± 56.32	109.5 ± 44.46	120.9 ± 25.94	200.2 ± 31.07	232.9 ± 48.99	350.0 ± 42.71
75	ER	25.6 ± 8.68	72.5 ± 14.08	370.4 ± 154.47	594.0 ± 103.28	518.6 ± 73.58	209.4 ± 52.91	184.4 ± 32.34	342.6 ± 35.45	639.1 ± 113.90
	SF	22.2 ± 6.07	86.1 ± 12.05	191.9 ± 36.30	301.3 ± 51.68	85.4 ± 35.29	122.2 ± 27.58	196.8 ± 36.70	238.4 ± 37.65	330.6 ± 39.50
100	ER	14.8 ± 4.26	41.3 ± 11.09	374.6 ± 168.58	632.1 ± 106.99	510.8 ± 82.95	219.9 ± 44.66	184.3 ± 24.53	391.7 ± 19.52	640.8 ± 114.74
	SF	16.6 ± 5.76	56.0 ± 12.87	218.0 ± 62.85	329.0 ± 49.67	101.9 ± 55.63	137.2 ± 30.98	196.6 ± 32.09	287.4 ± 58.90	316.4 ± 41.47

Table 7: Comparison of mean and standard deviation of SHD with increasing numbers of intervention sample sizes on ER and SF graphs with $D = 50$ in Figure 3.

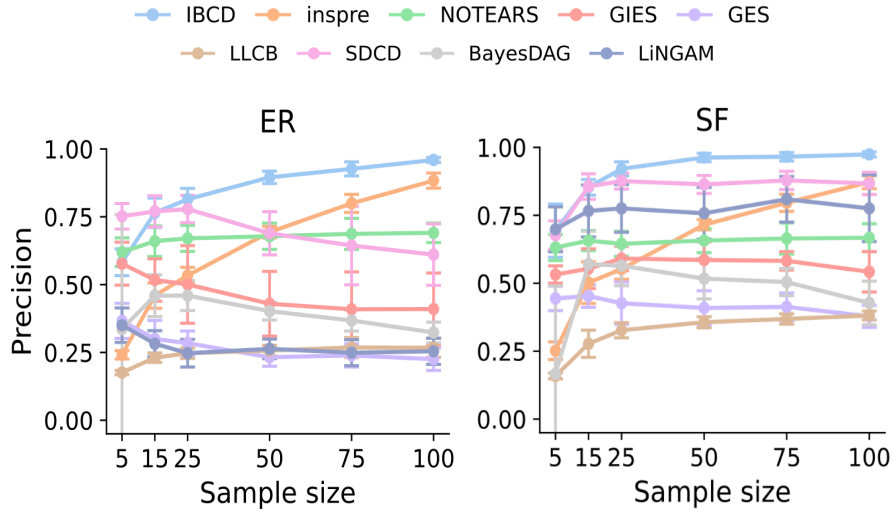


Figure 9: Comparison of precision with increasing numbers of intervention sample sizes on ER and SF graphs with $D = 50$.

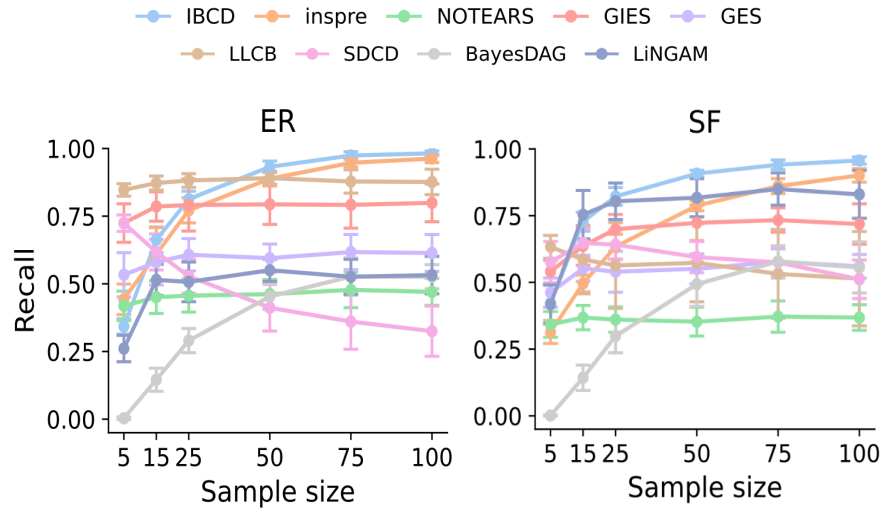


Figure 10: Comparison of recall with increasing numbers of intervention sample sizes on ER and SF graphs with $D = 50$.

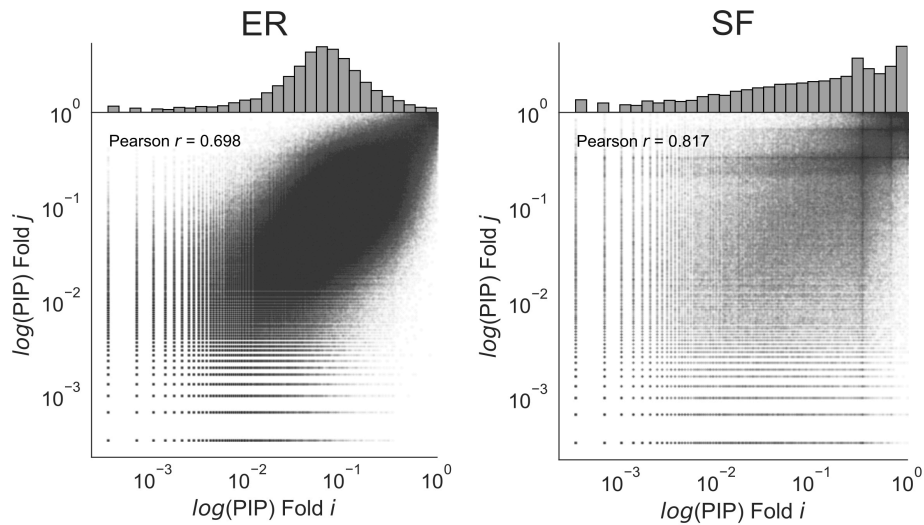


Figure 11: Agreement of log-transformed PIP across the ten cross-validation fold pairs on the K562 essential screen under ER and SF priors. Each point is one edge; the density of points forms a grey cloud. The positive correlation shows that high-PIP edges are consistently identified across folds.